Competitive spin-flipped normal reflection and equal-spin Andreev reflection in heterojunctions of nodal-line superconductors

Xiaohui Wang,[1,2] Hao Geng,[2] Wei Luo,[1,2,*] and Wei Chen[2,3,†]

[1]*School of Information Engineering, Jiangxi University of Science and Technology, Ganzhou 341000, China*
[2]*National Laboratory of Solid State Microstructures and School of Physics, Nanjing University, Nanjing 210093, China*
[3]*Collaborative Innovation Center of Advanced Microstructures, Nanjing University, Nanjing 210093, China*

(Received 10 November 2022; revised 22 April 2023; accepted 25 April 2023; published 8 May 2023)

The superconducting phase of topological semimetals has become a promising route for the implementation of topological superconductivity and non-Abelian Majorana fermions. Here, we investigate quantum transport in the junctions composed of a nodal-line superconductor, i.e., a topological nodal-line semimetal with superconducting pairing. It is shown that two topologically nontrivial regions exist in the surface Brillouin zone of the nodal-line superconductor labeled by the transverse momentum. Specifically, topological regions with topological invariants $\mathcal{N} = 1$ and $\mathcal{N} = 2$ host a single and a pair of Majorana zero modes at the surface, respectively. We show that the single Majorana zero mode in the $\mathcal{N} = 1$ region can induce resonant equal-spin Andreev reflection, while the Majorana pair in the $\mathcal{N} = 2$ region can lead to resonant spin-flipped normal reflection. Both reflection processes can give rise to spin currents but with different polarization directions, whose proportions can be adjusted by a Zeeman field. We also study the transport properties of the device with a sandwich structure and predict that strong crossed Andreev reflection can be implemented with a finite bias. Detection schemes for all these novel transport properties, which can be revealed by spin-resolved transport signatures, are proposed. Our work paves the way for the implementation and detection of Majorana fermions in nodal-line superconductors.

DOI: 10.1103/PhysRevB.107.195109

I. INTRODUCTION

A Majorana fermion (MF) is a fermion that is its own antiparticle. In condensed matter physics, the MF has been predicted to exist in topological superconductors as a quasiparticle excitation [1,2], which has attracted extensive research interest in the past decade for its non-Abelian braiding statistics and potential applications in fault-tolerant quantum computations [1–8]. The pursuit of MFs has ranged from intrinsic topological superconductors to hybridized systems [9,10], from one-dimensional (1D) to three-dimensional (3D) systems [11,12]. Recently, topological semimetals in the superconducting phase have become an important route for the implementation of MFs. For example, a Weyl-type topological superconductor can host a large number of Majorana zero modes on the surface, which are known as Majorana arcs connecting the nodal points in the surface Brillouin zone [13–15]. Another candidate is the nodal-line superconductor (NLSC), in which the drumheadlike Majorana zero modes emerge inside the projection of the nodal loops in the surface Brillouin zone [16–23].

The self-Hermiticity of MFs can give rise to a number of interesting physical phenomena, such as the fractional Josephson effect [24,25], resonant Andreev reflection (AR) [26,27], and half-integer conductance plateau [28,29]. For a single MF with a specific spin polarization, the so-called selective equal-spin AR can be induced [30–40]. In such a process, an electron with a proper spin direction denoted by **n** is resonantly reflected into a hole with the same spin. By contrast, electrons with the opposite spin polarization, $-\mathbf{n}$, are completely decoupled from the MF and cannot participate in the AR process. As such, a spin current can be generated by the equal-spin AR. It becomes particularly interesting if a huge number of Majorana zero modes exist, which can considerably enhance the relevant effect.

In this work, we investigate the transport properties of heterojunctions (in the z direction) composed of a NLSC, including both the normal metal (NM)-NLSC junction and the NM-NLSC-NM junction. At the interface of the junctions, Majorana zero modes with a very high degree of degeneracy emerge due to the band topology of the NLSC. By viewing the transverse momenta $k_{x,y}$ as parameters, the 3D NLSC can be understood as a bundle of 1D superconductors belonging to the BDI class [41,42]. In the (k_x, k_y) space or the surface Brillouin zone, three topologically distinct regions exist, with the invariants being $\mathcal{N} = 0$, 1, and 2, with $\mathcal{N}$ also being the number of MFs on the surface. We show that both the nontrivial phases with $\mathcal{N} = 1$ and 2 can lead to interesting spin-resolved transport phenomena in the NM-NLSC junction. Specifically, for the $\mathcal{N} = 1$ phase, all the MFs couple to the electrons in the NM with their spin pointing in the $-y$ direction and induce the equal-spin AR [30], which thus generates a giant spin current. For the $\mathcal{N} = 2$ phase, the two MFs suppress the AR process due to destructive interference. Instead, electron

*jxluow@163.com
†pchenweis@gmail.com

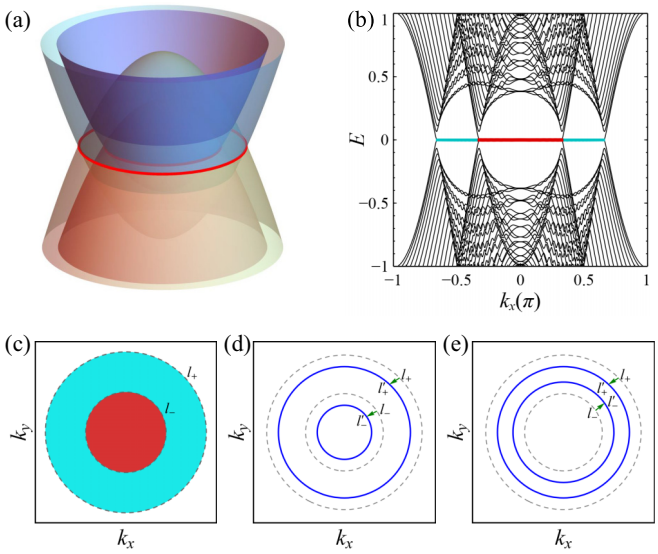

FIG. 1. (a) Sketch of the band structure of a NLSC for $k_z = 0$. The conduction and valance bands cross at the two red circles. (b) Energy spectrum of a 1D NLSC as a function of k_x at $k_y = 0$. The lattice model is constructed by the substitution $k_z \to a^{-1} \sin k_z a$, $k^2_{0,x,z} = 2a^{-2}(1 - \cos k_{0,x,y} a)$, with a being the lattice constant. (c) Phase diagram determined by the topological invariant $\mathcal{N}$ in the surface Brillouin zone. The phase boundaries are a projection of the nodal loops onto the surface Brillouin zone. The effect of (d) the z direction and (e) x direction Zeeman fields on the phase diagram.

transport is dominated by the resonant spin-flipped normal reflection [43], in which an incident electron with its spin direction perpendicular to the y axis is reflected with spin reversal. Both topologically nontrivial regions can generate spin currents, but their spin polarizations are different. It is shown that a Zeeman field can effectively tune the areas of the topological regions in the surface Brillouin zone and thus the proportion of the two competitive scattering processes. For the NM-NLSC-NM junction, we find that strong crossed AR can be implemented with finite bias. We also show that the aforementioned unique effects can be detected by spin-resolved transport schemes with the proposed devices.

II. MODEL

In the Nambu basis $(c_{\mathbf{k}\uparrow}, c_{\mathbf{k}\downarrow}, c^\dagger_{-\mathbf{k}\uparrow}, c^\dagger_{-\mathbf{k}\downarrow})$, the Hamiltonian of a NLSC can be written as [19]

$$H = B\left(k_0^2 - |\mathbf{k}|^2\right)\sigma_z\tau_z + \lambda k_z \sigma_x \tau_0 + \Delta\sigma_y\tau_y, \qquad (1)$$

where $c_{\mathbf{k}\uparrow}$ ($c_{\mathbf{k}\downarrow}$) denotes a spin-up (-down) electron with momentum $\mathbf{k}$, $|\mathbf{k}|^2 = k_x^2 + k_y^2 + k_z^2$ is the total momentum squared, and σ_i and τ_i are the Pauli matrices acting on the spin and particle-hole space. The energy spectra are $E_{s,\pm} = s\sqrt{[B(k_0^2 - |\mathbf{k}|^2) \pm \Delta]^2 + \lambda^2 k_z^2}$, with $s = \pm 1$ standing for conduction and valence bands. The four bands cross at two nodal rings $l_\pm$ with radii $k_\pm = \sqrt{k_0^2 \pm \Delta/B}$ in the $k_z = 0$ plane [see Fig. 1(a)]. Considering the transverse momentum $\mathbf{k}_\parallel = (k_x, k_y)$ as a parameter, the Hamiltonian (1) can map to a 1D Hamiltonian in the z direction. For a fixed $\mathbf{k}_\parallel$, the 1D Hamiltonian $H(k_z)$ belongs to a BDI class topological superconductor [41,42], which satisfies the time-reversal-like symmetry $\mathcal{T}H(k_z)\mathcal{T}^{-1} = H(-k_z)$ and particle-hole symmetry $\mathcal{P}H(k_z)\mathcal{P}^{-1} = -H(-k_z)$, so the chiral symmetry $\mathcal{C}H(k_z)\mathcal{C}^{-1} = -H(k_z)$, where $\mathcal{T} = i\sigma_y\tau_y\mathcal{K}$, $\mathcal{P} = \sigma_0\tau_x\mathcal{K}$, and $\mathcal{C} = \mathcal{T}\mathcal{P}$, with $\mathcal{K}$ being the complex conjugate operator. A BDI class topological superconductor is classified by an integer topological invariant $\mathcal{N}$ [41,42], which denotes the number of topological protected MFs at each end of the 1D superconducting wire.

One can obtain the phase diagram on the surface Brillouin zone by calculating the topological invariant $\mathcal{N}$ [44,45]. As expected, the two nodal loops $l_\pm$ are the phase boundaries that divides the k_x-k_y plane into three topological phases [see Fig. 1(c)]. Inside the small loop l_-, the topological invariant $\mathcal{N} = 2$, indicating that there are two MFs at the end of the system. When $k_\parallel$ increases, one of the two MFs in $\mathcal{N} = 2$ is annihilated, and a new $\mathcal{N} = 1$ phase with a single MF emerges. When $k_\parallel > k_+$, the phase $\mathcal{N} = 0$ is trivial with no MF.

In Fig. 1(b), we plot the energy spectrum of the 1D NLSC at an open boundary. For $\mathcal{N} = 2$ (1), the red (cyan) lines are fourfold (doubly) degenerate, denoting two (a single) zero modes at each end. Moreover, one can confirm that these zero modes are MFs by analytically solving $H(-i\partial_z)\Psi_{\rm SC}(z) = 0$. We consider the system to occupy the half-space $z \geqslant 0$. Using the trial function $\Psi_{\rm SC}(z) = |\phi\rangle e^{\xi z}$, the secular equation gives eight roots $\pm\xi_{1,2,3,4}$, with $\xi_{1,2,3,4} = |\frac{\lambda \pm \sqrt{\lambda^2 + 4B[-B(k_0^2 - k_\parallel^2) \pm \Delta]}}{2B}|$. Because the wave function is finite, ξ can take only the four negative values. Consequently, the general solution is given by $\Psi_{\rm SC}(z) = \sum_{i=1}^4 s_i |\phi_i\rangle e^{-\xi_i z}$. In the $\mathcal{N} = 2$ phase where $B(k_0^2 - k_\parallel^2) > \Delta$, one can obtain $|\phi_1\rangle = |\phi_2\rangle = (ie^{-i\frac{\pi}{4}}, -e^{-i\frac{\pi}{4}}, -ie^{i\frac{\pi}{4}}, -e^{i\frac{\pi}{4}})^T$ and $|\phi_3\rangle = |\phi_4\rangle = (ie^{i\frac{\pi}{4}}, -e^{i\frac{\pi}{4}}, -ie^{-i\frac{\pi}{4}}, -e^{-i\frac{\pi}{4}})^T$, with $\xi_{1,2} = \frac{\lambda \pm \sqrt{\lambda^2 + 4B[-B(k_0^2 - k_\parallel^2) - \Delta]}}{2B}$ and $\xi_{3,4} = \frac{\lambda \pm \sqrt{\lambda^2 + 4B[-B(k_0^2 - k_\parallel^2) + \Delta]}}{2B}$. Imposing the open boundary condition $\Psi_{\rm SC}(0) = 0$, we have $s_1 = -s_2$ and $s_3 = -s_4$; then the wave function is $\Psi_{\mathcal{N}=2} = \gamma_1 + \gamma_2$, with $\gamma_1 = |\phi_1\rangle e^{-\xi_1 z} - |\phi_2\rangle e^{-\xi_2 z}$ and $\gamma_2 = |\phi_3\rangle e^{-\xi_3 z} - |\phi_4\rangle e^{-\xi_4 z}$. It is clear that they describe two MFs since $\gamma_{1,2} = \gamma^\dagger_{1,2}$. When $\mathcal{N} = 1$, $|B(k_0^2 - k_\parallel^2)| < \Delta$, $|\phi_{3,4}\rangle = (ie^{\mp i\frac{\pi}{4}}, \pm e^{\mp i\frac{\pi}{4}}, -ie^{\pm i\frac{\pi}{4}}, -e^{\pm i\frac{\pi}{4}})^T$. Because $|\phi_3\rangle \neq |\phi_4\rangle$, the boundary condition can be satisfied only for coefficients $s_3 = s_4 = 0$, so the wave function is $\Psi_{\rm SC}(0) = \gamma_1$, indicating only one MF end state. Last, for the $\mathcal{N} = 0$ phase, $|\phi_{1,2}\rangle$ change to $|\phi_{1,2}\rangle = (ie^{\mp i\frac{\pi}{4}}, \mp e^{\mp i\frac{\pi}{4}}, -ie^{\pm i\frac{\pi}{4}}, \mp e^{\pm i\frac{\pi}{4}})^T$. Now the four spinors $|\phi_{1,2,3,4}\rangle$ are not equal; $\Psi_{\rm SC}(0) = 0$ requires all the coefficients $s_i = 0$, so no bound state exists.

A MF will induce equal-spin AR; specifically, for the $\mathcal{N} = 1$ phase here, each MF couples to the electron with spin pointing in the $-y$ direction [19,31], so the $\mathcal{N} = 1$ phase induces a spin-polarized current. For the $\mathcal{N} = 2$ phase, the AR is completely suppressed because of the destructive interference between the local AR amplitudes caused by the two MFs [19,31]. However, if we examine the spin transport as shown below, we can find that the two MFs will induce resonant spin-flipped reflection; for example, a spin-up electron will be reflected as a spin-down electron. Thus, a spin current will also be induced because the incident and reflected electrons have opposite spin polarizations. We can see that both phases induce spin currents, but the spin polarizations are different.

In order to tune the spin currents, we apply a Zeeman field described by

$$H_Z = V_x\sigma_x\tau_z + V_z\sigma_z\tau_z. \tag{2}$$

The energy spectra in the presence of the Zeeman field are $E_s = s\sqrt{\Gamma_{xz}^2 + \Delta^2 + \lambda^2 k_z^2 \pm 2\sqrt{\Gamma_{xz}^2\Delta^2 + V_x^2\lambda^2 k_z^2}}$, with $\Gamma_{xz}^2 = V_x^2 + [V_z + B(k_0^2 - |\mathbf{k}|^2)]^2$. We can see that when $V_x < \Delta$, the nodal loops are modified to $l'_\pm$ in the $k_z = 0$ plane with radii $k'_\pm = \sqrt{k_0^2 + (V_z \pm \sqrt{\Delta^2 - V_x^2})/B}$. Now the nodal loops $l'_\pm$ serve as the new critical lines dividing different topological phases. Therefore, we can achieve a topological transition by applying Zeeman fields along the x and z directions. Specifically, V_z causes the inner and outer circles to change synchronously, keeping the squared difference of their radii constant [see Fig. 1(d)], while V_x makes the two circles move closer to each other [see Fig. 1(e)]. Particularly, when $V_x \geqslant \Delta$, the difference between the radii of the two circles is zero, so the topological phase $\mathcal{N} = 1$ disappears; then only the nontrivial resonant spin-flipped reflection exists. It is noted that although, in the (k_x, k_y) space, the energy gap is always open when $V_x > \Delta$, the topological transition can happen without the energy gap closing [46,47]. Calculating the topological invariant, we find that when $\sqrt{V_x^2 - \Delta^2} < \lambda\sqrt{\frac{V_z + B(k_0^2 - k_\parallel^2)}{B}}$, $\mathcal{N} = 2$; otherwise, $\mathcal{N} = 0$. When $V_x < \Delta$ and $V_z < -Bk_0^2 + \sqrt{\Delta^2 - V_x^2}$, the radius of the inner circle is less than zero, so the $\mathcal{N} = 2$ phase disappears, and only the $-y$ direction spin-polarized current will appear.

III. SPIN-DEPENDENT TRANSPORT IN A NM-NLSC JUNCTION

In order to investigate the spin-dependent transport in a NM-NLSC junction, we employ the Bogoliubov–de Gennes (BdG) equation [48]. A semi-infinite NM lead is attached to the left end of the NLSC. Here, the incident energy is set to $E = 0$. The solution of the BdG equation in the NLSC is

$$\Psi_{\mathrm{SC}}(z) = \sum_{i=1}^{4} s_i|\phi_i\rangle e^{ik_{zi}z}, \tag{3}$$

with $|\phi_i\rangle = [1, b_i, c_i, d_i]^T$, $b_i = \frac{2\lambda k_{zi}(\Gamma_z - Bk_{zi}^2)}{(\Gamma_z - Bk_{zi}^2)^2 - \lambda^2 k_{zi}^2 - \Delta^2 + V_x^2}$, $c_i = \frac{-\lambda k_{zi} - V_x + (\Gamma_z - Bk_{zi}^2)b_i}{\Delta}$, $d_i = \frac{(\Gamma_z - Bk_{zi}^2) + (\lambda k_{zi} + V_x)b_i}{\Delta}$, and $\Gamma_z = V_z + B(k_0^2 - k_\parallel^2)$, with k_{zi} being the roots of the eigenequation $|H| = 0$ with positive imaginary parts which make the wave functions decay into the NLSC.

Assuming that the lead is described by the Hamiltonian $H_{\mathrm{L}} = (C|\mathbf{k}|^2 - \mu)\sigma_0\tau_z$, the wave function in the lead at the Fermi energy can be written as $\Psi_{\mathrm{L}}(z) = e^{ik_{\mathrm{F}}z}|e_1\rangle + r_{e\uparrow}^{e\uparrow}e^{-ik_{\mathrm{F}}z}|e_1\rangle + r_{e\uparrow}^{e\downarrow}e^{-ik_{\mathrm{F}}z}|e_2\rangle + r_{e\uparrow}^{h\uparrow}e^{ik_{\mathrm{F}}z}|h_1\rangle + r_{e\uparrow}^{h\downarrow}e^{ik_{\mathrm{F}}z}|h_2\rangle$, where k_{F} is the Fermi wave vector and $|e_1\rangle = (1, 0, 0, 0)^T$, $|e_2\rangle = (0, 1, 0, 0)^T$, $|h_1\rangle = (0, 0, 1, 0)^T$, and $|h_2\rangle = (0, 0, 0, 1)^T$. Here, $r_{e\sigma}^{\alpha\sigma'}$ denotes the amplitude for an incoming electron with spin σ to be reflected as an α particle with spin σ', where α denotes an electron or hole. All the scattering

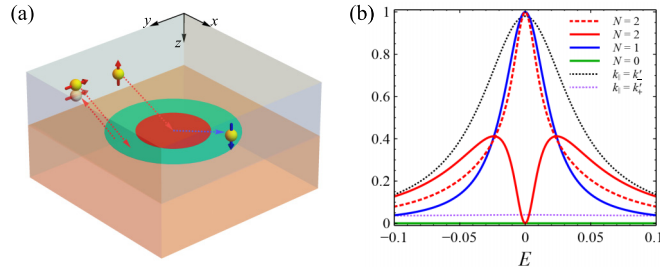

FIG. 2. (a) When the transverse momentum lies inside the cyan region where $\mathcal{N} = 1$, incident electrons with spin antiparallel to the y axis will undergo equal-spin AR in which an electron is reflected as a hole with the same spin. When the transverse momentum lies inside the red region where $\mathcal{N} = 2$, incident electrons with spin perpendicular to the y axis will undergo spin-flipped normal reflection. (b) The reflection probabilities as a function of incident energy. The solid lines are the AR probabilities; the red, blue, and green lines correspond to the phases $\mathcal{N} = 2$, 1, and 0, respectively. The dashed line is the spin-flipped reflection probability in the $\mathcal{N} = 2$ phase. The dotted lines are the AR probabilities at the nodal lines. The parameters are $B = C = 1$, $V_x = V_z = 0$, $\Delta = 1$, $\lambda = 0.2$, and $k_{\mathrm{F}} = 5k_0 = 20$.

coefficients can be solved by boundary conditions:

$$\Psi_{\mathrm{L}}(0) = \Psi_{\mathrm{SC}}(0) = \Psi(0),$$
$$C\tau_z\Psi'_{\mathrm{L}}(0) + B\sigma_z\tau_z\Psi'_{\mathrm{SC}}(0) = \frac{i}{2}\lambda\sigma_x\Psi(0). \tag{4}$$

It is noted that the wave function (3) can be simplified for a fixed topological phase. We first consider the case of $\mathcal{N} = 1$, in which a MF is localized at the boundary for a given $\mathbf{k}_\parallel$ and the equal-spin AR can be induced. In this phase, we have $|\Gamma_z| < \sqrt{\Delta^2 - V_x^2}$, and the wave functions are simplified as $|\phi_1\rangle = |\phi_2\rangle = (ie^{-i\varphi}, -e^{-i\varphi}, -ie^{i\varphi}, -e^{i\varphi})^T$, $|\phi_3\rangle = (ie^{-i\varphi}, e^{-i\varphi}, -ie^{i\varphi}, -e^{i\varphi})^T$, and $|\phi_4\rangle = (ie^{i\varphi}, -e^{i\varphi}, -ie^{-i\varphi}, -e^{-i\varphi})^T$, with $2\varphi = \arccos(V_x/\Delta)$, and the corresponding wave vectors are $k_{z1,2} = i\frac{\lambda \pm \sqrt{\lambda^2 + 4B(-\Gamma_z - \sqrt{\Delta^2 - V_x^2})}}{2B}$ and $k_{z3,4} = i\frac{\mp\lambda + \sqrt{\lambda^2 + 4B(-\Gamma_z + \sqrt{\Delta^2 - V_x^2})}}{2B}$. The normal reflection and AR matrices, which relate the incoming electron $(c_{k\uparrow}, c_{k\downarrow})$ to the outgoing electrons $(c_{k\uparrow}, c_{k\downarrow})$ and holes $(c^\dagger_{-k\uparrow}, c^\dagger_{-k\downarrow})$, are

$$r_{ee} = \frac{1}{2}\begin{pmatrix} 1 & -i \\ i & 1 \end{pmatrix}, \quad r_{he} = \frac{1}{2}\begin{pmatrix} -i & 1 \\ 1 & i \end{pmatrix}. \tag{5}$$

Denoting $|-\rangle = \frac{1}{\sqrt{2}}(1, -i)^T$, we have $r_{he}|-\rangle = [1^*, (-i)^*]^T = |+\rangle$ and $r_{ee}|-\rangle = 0$. The reflected hole with spinor $[1^*, (-i)^*]^T$ is created due to missing electrons with spinor $(1, -i)^T$ below the Fermi energy. Consequently, a pair of electrons with spin parallel to $\mathbf{n} = \langle -|\boldsymbol{\sigma}|-\rangle = (0, -1, 0)$ is injected into the NLSC in each tunneling event, resulting in equal-spin AR [see Fig. 2(a)]. On the contrary, the electrons with spinor $|+\rangle$, whose spins are antiparallel to $\mathbf{n}$, are totally reflected as electrons with unchanged spin since $r_{ee}|+\rangle = |+\rangle$.

It is worth noting that the scattering matrices (5) are constant matrices, independent of the material parameters and wave vectors, indicating that each MF couples electrons of the same spin. This is an important property of NLSCs. In

general, the spins of MFs' coupled electrons are different, depending on the material properties [30,33]. For example, in Ref. [33], the spins of MFs on the Majorana flat band coupled electrons are not exactly the same, depending on the wave vectors, which greatly reduce the spin current. In contrast, for the present case, the polarizations of the spin currents generated by all the MFs in the phase $\mathcal{N}=1$ are the same, along the $-y$ direction, and are insensitive to material details. This is beneficial for generating giant spin current and makes the NLSC a candidate for spintronic applications.

In the regime with $\mathcal{N}=2$, where $\Gamma_z > \sqrt{\Delta^2 - V_x^2}$, the wave functions are simplified as $|\phi_1\rangle = |\phi_2\rangle = (ie^{-i\varphi}, -e^{-i\varphi}, -ie^{i\varphi}, -e^{i\varphi})^T$ and $|\phi_3\rangle = |\phi_4\rangle = (ie^{i\varphi}, -e^{i\varphi}, -ie^{-i\varphi}, -e^{-i\varphi})^T$, and the corresponding wave vectors are $k_{z1,2} = i\frac{\lambda \pm \sqrt{\lambda^2 + 4B(-\Gamma_z - \sqrt{\Delta^2 - V_x^2})}}{2B}$ and $k_{z3,4} = i\frac{\lambda \pm \sqrt{\lambda^2 + 4B(-\Gamma_z + \sqrt{\Delta^2 - V_x^2})}}{2B}$. We obtain the scattering matrices

$$r_{ee} = \begin{pmatrix} 0 & -i \\ i & 0 \end{pmatrix}, \quad r_{he} = 0. \tag{6}$$

We can see that for the phase $\mathcal{N}=2$, although there are two MF end states, the AR is completely suppressed [19,31]. However, the normal reflection matrix r_{ee} indicates that the two MFs induce nontrivial spin transport. Considering an electron $|\mathbf{n}_\perp\rangle = (\cos\frac{\theta}{2}, \sin\frac{\theta}{2})^T$ with spin pointing in the direction $\mathbf{n}_\perp = (\sin\theta, 0, \cos\theta)$ incident from the NM, we see that it will be totally reflected as an electron $r_{ee}|\mathbf{n}_\perp\rangle = (i\sin\theta, -i\cos\theta)^T$ whose spin is antiparallel to $\mathbf{n}_\perp$ [see Fig. 2(a)]. Therefore, the two MFs induce a resonant spin-flipped reflection for electrons with spin perpendicular to the y direction. The resonant spin-flipped reflection has been studied in nodal-line semimetals [43], in which the topological nontrivial phase is equivalent to the $\mathcal{N}=2$ phase here.

Finally, let us look at the case of $\mathcal{N}=0$, for which $\Gamma_z < -\sqrt{\Delta^2 - V_x^2}$ and the wave functions are simplified as $|\phi_1\rangle = (ie^{-i\varphi}, -e^{-i\varphi}, -ie^{i\varphi}, -e^{i\varphi})^T$, $|\phi_2\rangle = (ie^{i\varphi}, e^{i\varphi}, -ie^{-i\varphi}, e^{-i\varphi})^T$, $|\phi_3\rangle = (ie^{-i\varphi}, e^{-i\varphi}, -ie^{i\varphi}, -e^{i\varphi})^T$, and $|\phi_4\rangle = (ie^{i\varphi}, -e^{i\varphi}, -ie^{-i\varphi}, -e^{-i\varphi})^T$. It is easy to obtain the normal reflection $r_{e\uparrow}^{e\uparrow} = r_{e\downarrow}^{e\downarrow} = 1$, while other reflection amplitudes are zero. The transport is trivial.

In Fig. 2(b) we show the reflection probabilities as a function of energy. As expected, in the phase $\mathcal{N}=1$, the zero-bias AR probability is 1 due to the MF-induced resonant AR. When $\mathcal{N}=2$, the zero-bias AR probability is zero, showing a zero-bias dip. Although the AR is suppressed by the interference of the two MFs, a resonant spin-flipped normal reflection is induced. The spin-flipped reflection probability exhibits a resonant peak instead of the AR dip at zero energy (see the red dashed line). In addition, the AR probabilities at the two nodal lines are also plotted.

The above nontrivial spin transports are the result of MFs, which are insensitive to material details. In the weak-coupling limit, we can get the same results with a tunneling Hamiltonian description, which makes it easier to see the effect of MFs. In the tunneling limit, we can use a tunneling Hamiltonian to describe the coupling between the MFs and the NM. The wave functions of MFs $\gamma_{1,2}$ are given in Sec. II; one can find that in the presence of the Zeeman field by substitution $\pi/4 \to \varphi$ and $-\xi_i \to ik_{zi}$. The effective Hamiltonian can be written as

$$\begin{aligned} H_{\text{eff}} &= H_{\text{L}} + H_{\text{T}}, \\ H_{\text{L}} &= iv_{\text{F}} \int_{-\infty}^{\infty} [\psi_{\mathbf{k}\uparrow}^\dagger(z)\partial_z\psi_{\mathbf{k}\uparrow}(z) + \psi_{\mathbf{k}\uparrow}^\dagger(z)\partial_z\psi_{\mathbf{k}\uparrow}(z)]dz, \\ H_{\text{T}} &= t_1\gamma_1[ie^{-i\varphi}\psi_{\mathbf{k}\uparrow} - e^{-i\varphi}\psi_{\mathbf{k}\downarrow} + ie^{i\varphi}\psi_{\mathbf{k}\uparrow}^\dagger + e^{i\varphi}\psi_{\mathbf{k}\downarrow}^\dagger] \\ &\quad + t_2\gamma_2[ie^{i\varphi}\psi_{\mathbf{k}\uparrow} - e^{i\varphi}\psi_{\mathbf{k}\downarrow} + ie^{-i\varphi}\psi_{\mathbf{k}\uparrow}^\dagger + e^{-i\varphi}\psi_{\mathbf{k}\downarrow}^\dagger], \end{aligned} \tag{7}$$

where H_{L} describes the NM with spin-up and spin-down electrons $\psi_{\mathbf{k}\uparrow,\downarrow}$ and Fermi velocity v_{F} and H_{T} describes the coupling between MFs and the NM, with $t_{1,2}$ being the coupling amplitudes. The scattering matrix can be calculated using the equation of motion approach [26]. It can be shown that the scattering matrices for an incoming electron with energy E are

$$r_{ee} = Z^{-1}\begin{pmatrix} 1 - iA_1 & A_1 \\ -A_1 & 1 - iA_1 \end{pmatrix}$$

and

$$r_{he} = Z^{-1}\begin{pmatrix} -iA_2 & A_2 \\ A_2 & iA_2 \end{pmatrix},$$

where $Z = (E + i2\zeta_1)(E + i2\zeta_2) + 4\zeta_1\zeta_2\cos^2 2\varphi$, $A_1 = \zeta_1(E + i2\zeta_2) + \zeta_2(E + i2\zeta_1) - i4\zeta_1\zeta_2\cos^2 2\varphi$, and $A_2 = \zeta_1(E + i2\zeta_2)e^{2i\varphi} + \zeta_2(E + i2\zeta_1)e^{-2i\varphi} - i4\zeta_1\zeta_2\cos 2\varphi$, with $\zeta_{1,2} = 2\pi t_{1,2}^2$. At $E=0$, we have $r_{he}(E=0) = 0$ and

$$r_{ee}(E=0) = \begin{pmatrix} 0 & -i \\ i & 0 \end{pmatrix}$$

as long as both t_1 and t_2 are nonvanishing, indicating that the suppressed ARs and resonant spin-flipped reflection are the results of interference of two MFs. When $t_2 = 0$ in the $\mathcal{N}=1$ phase, we have

$$r_{he}(E=0) = \frac{1}{2}\begin{pmatrix} 1 & -i \\ i & 1 \end{pmatrix},$$

which is consistent with the result in Eq. (5).

In the above calculation, it is shown that for the $\mathcal{N}=1$ phase, all the MFs couple to the electrons with spin pointing in the $-y$ direction and induce the equal-spin AR, resulting in spin currents with the exact same spin polarization. For the $\mathcal{N}=2$ phase, although the ARs are completely suppressed, the two MFs for a given $\mathbf{k}_\parallel$ induce a resonant spin-flipped reflection for electrons with spin perpendicular to the y axis. The polarizations of the spin currents induced by the two nontrivial phases are different. We can tune the spin currents with different polarization directions by a Zeeman field.

By the summation of scattering probabilities over $\mathbf{k}_\parallel$, one can obtain the zero-bias differential spin conductance of the NM-NLSC junction. The $\mathcal{N}=1$ states appear in the regime in which $k'_- < |\mathbf{k}_\parallel| < k'_+$. So the differential spin conductance is

$$G_s^{-\mathbf{y}} = \frac{2e^2}{h}\sum_{\mathbf{k}_\parallel} \text{Tr}(r_{he}r_{he}^\dagger) = \frac{2e^2}{h}\frac{S(k_+'^2 - k_-'^2)}{4\pi}, \tag{8}$$

with S being the cross-section area of the NLSC and the superscript representing the polarization direction of the spin

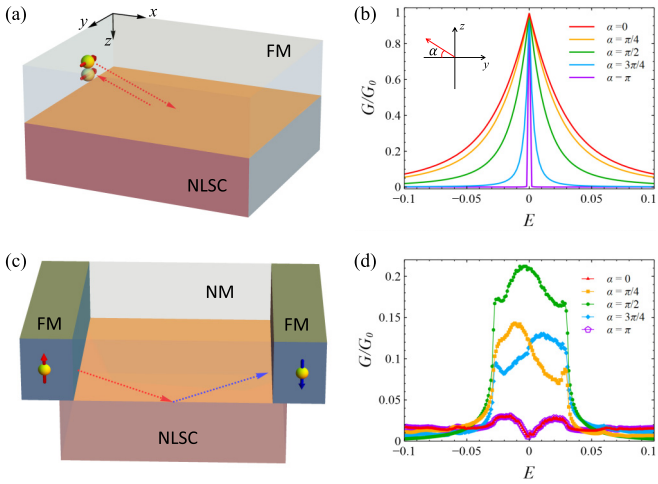

FIG. 3. (a) and (c)The setups for probing the equal-spin AR and resonant spin-flipped reflection, respectively. (b) and (d) The conductances of setups in (a) and (c), respectively. We take $V_z = -Bk_0^2 + \Delta$ and $k_F = 1.1k'_+$ in (b) and $V_z = 0$ and $k_F = 1.1k_0$ in (d). Other parameters are set to $B = C = 1$, $\Delta = 1$, $\lambda = 0.2$, $k_0 = 2.5$, and $V_x = 0$. $G_0 = (Sk_F^2/4\pi)(e^2/\hbar)$ is the single conductance of the electrode.

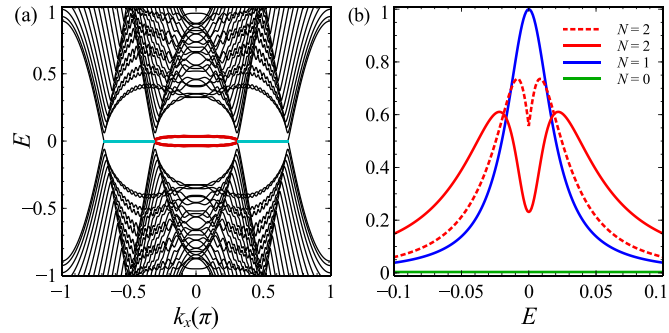

FIG. 4. (a) Energy spectrum of a 1D NLSC as a function of k_x at $k_y = 0$ in the presence of a finite potential μ_0. (b) The reflection probabilities as a function of incident energy. The chemical potential is set to $\mu_0 = 0.5$, and other parameters are the same as those in Fig. 2.

current. For the transport of the $\mathcal{N} = 2$ phase, we consider that a ferromagnet is coupled to a section of the NM so that electrons passing through the magnetic section are strongly polarized by the ferromagnet. By tuning the magnetization direction of the ferromagnet, we can control the spin polarization direction of the incident electrons at the NM-NLSC junction. When the spin polarization direction lies in the x-z plane, the resonant spin-flipped reflection occurs. The differential spin conductance is given by

$$G_s^{\mathbf{n}_\perp} = \frac{e^2}{h}\sum_{\mathbf{k}_\parallel}(1 + |r_f|^2 - |r_c|^2) = \frac{2e^2}{h}\frac{Sk'^2}{4\pi}, \qquad (9)$$

where r_f and r_c are the spin-flipped and spin-conserved reflection amplitudes, respectively.

The spin transports in the two nontrivial phases can be detected by charge currents using ferromagnetic metals (FMs) as electrodes. In the $\mathcal{N} = 1$ phase only electrons with spin pointing in the $-y$ direction can undergo equal-spin AR, so if a ferromagnet is used as an electrode, the conductance of a NM-NLSC junction depends on the spin polarization of the lead. For simplicity, we assume that the polarization direction of the ferromagnet is in the y-z plane and denote the polarization angle of the ferromagnet with respect to the $-y$ direction as α. The conductance of the NM-NLSC junction for different angles α is shown in Fig. 3(b). When $\alpha = 0$, all the incident electrons undergo equal-spin AR, so the width of the conductance peak is wide. As α deviates from zero, the incident electrons can be decomposed into the AR channel and total reflection channel. The width of the conductance peak becomes narrow as α increases owing to the weight of the total reflection channel becoming more important. The height of the zero-bias conductance peak is not changed due to the resonant AR.

The spin-flipped reflection can be probed using the setup in Fig. 3(c) [43], in which the polarizations of the ferromagnets are taken to be antiparallel and transport through the device is possible only due to spin-flipping processes. The differential conductance of such a setup can be calculated based on the lattice model using the KWANT package [49]. From Eq. (6), it is found that the electrons with spin perpendicular to the y direction are totally reflected as electrons with opposite spin, whereas electrons with spin parallel and antiparallel to the y direction are totally reflected as electrons with unchanged spin. Thus, when the spin polarization is pointing to the z axis, the conductance peak is the highest, as shown by the green line in Fig. 3(d). As the polarization direction deviates from the z axis, the zero-bias conductance decreases. When the polarization direction is along the y axis, the zero-bias conductance is zero.

From the above discussions, one can see that the charge conductances in the setups in Figs. 3(a) and 3(c) are sensitively dependent on the polarization direction of the FMs. Therefore, using FMs, we can detect the spin transports and distinguish the polarization directions of the spin currents in phases $\mathcal{N} = 1$ and $\mathcal{N} = 2$ from the dependence of charge conductances on α. Our detection scheme is feasible in experiment. The FM-superconductor junction in Fig. 3(a) is widely used to detect spin polarization of electrons in metals [50] and the order parameter of unconventional superconductors [51,52]. The superconductor-metal junction in Fig. 3(c) is also a common setup for the study of the AR process [53].

In the above calculation, we considered a special chemical potential which locates at the sweet point satisfying the neutrality condition and so guarantees chiral symmetry. Now we discuss the effect of a finite chemical potential, which is modeled by $\mu_0\tau_z$. This term breaks the time-reversal-like symmetry $\mathcal{T}$ and chiral symmetry $\mathcal{C}$. In this case, the degeneracy of the two MFs in phase $\mathcal{N} = 2$ is split, and the zero modes are gapped [see Fig. 4(a)] since the chemical potential gives rise to a coupling between the MFs. As a result, the transport properties of the $\mathcal{N} = 2$ phase are greatly changed. We show the reflection probabilities as a function of energy in Fig. 4(b). We can see that the zero-energy resonant peak of spin-flipped reflection drops because the double degeneracy of the Majorana zero modes is split. Meanwhile, the complete interference cancellation of the two MFs is removed, giving a nonvanishing AR.

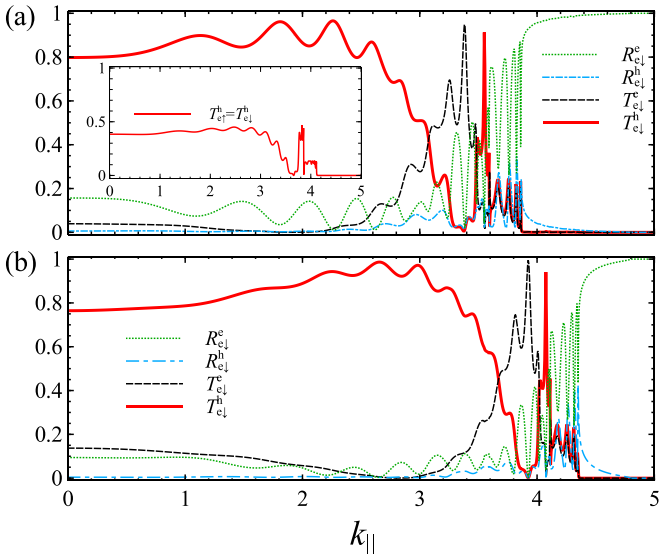

FIG. 5. Probabilities of various tunneling processes as a function of the transverse wave vector $k_\parallel$ for (a) spin-up electron incidence and (b) spin-down electron incidence. The incident energy is set to $E = 2$, and other parameters are $B{=}C{=}1$, $\Delta{=}1$, $k_F = 1.25k_0 = 5$, $\lambda = 0.2$, and $L = 10$.

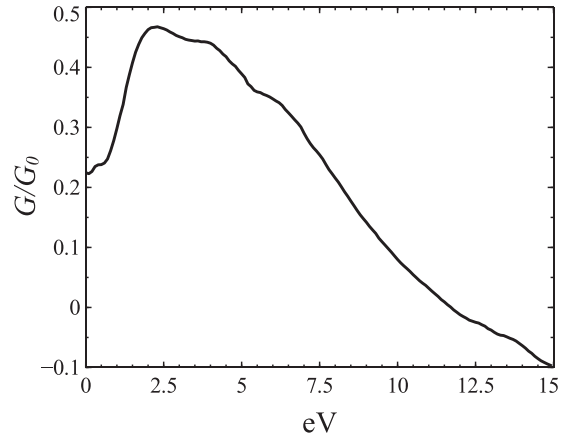

FIG. 6. The total nonlocal conductance as a function of voltage bias. Other parameters are the same as those in Fig. 5.

IV. CROSSED ANDREEV REFLECTION

Next, we consider a NM-NLSC-NM junction where the crossed Andreev reflection (CAR) process can occur, in which the incident electron and the Andreev reflected hole are in different terminals. The zero-bias transport of a NM-NLSC-NM was investigated in Refs. [19,31], which found that in the $\mathcal{N} = 2$ phase, the two MFs can strongly enhance the CAR. Nevertheless, the sum of the CAR probabilities of the two spin channels is always less than 1, because at zero bias the spin state $|+\rangle$ is decoupled from the MF and is totally reflected as an electron. This spin transport property is determined by the wave function of the NLSC, which is energy dependent. We expect that when the incident energy is not zero, the CAR can be enhanced because both spin states $|+\rangle$ and $|-\rangle$ participate in it.

Here, we concentrate instead on the CAR under finite bias. In such a junction, the wave function in the NLSC is

$$\psi_{SC}(z) = \sum_{i=1}^{8} s_i |\phi_i\rangle e^{ik_{zi}z}, \tag{10}$$

where $|\phi_i\rangle$ are the same as those in Eq. (3) and k_{zi} are the eight roots of the eigenequation $|H - E| = 0$. Note that all eight roots are needed because the NLSC is in the middle of the junction and is finite. The incident wave function in the left lead is the same as in the NM-NLSC, and the outgoing wave function in the right lead is $\Psi_R(z) = t^{e\uparrow}_{e\uparrow} e^{-ik_F z}|e_1\rangle + t^{e\downarrow}_{e\uparrow} e^{-ik_F z}|e_2\rangle + t^{h\uparrow}_{e\uparrow} e^{ik_F z}|h_1\rangle + t^{h\downarrow}_{e\uparrow} e^{ik_F z}|h_2\rangle$, where $t^{e\uparrow}_{e\uparrow}$ and $t^{e\downarrow}_{e\uparrow}$ are the transmission amplitudes and $t^{h\downarrow}_{e\uparrow}$ and $t^{h\downarrow}_{e\uparrow}$ are the CAR amplitudes. One can obtain the transport coefficients using the boundary conditions at $z = 0$ and L.

There are four tunneling processes, consisting of normal reflection, elastic cotunneling, local AR, and CAR, with the probabilities given by $R^e_{e\sigma} = |r^{e\sigma}_{e\sigma}|^2 + |r^{e\bar{\sigma}}_{e\sigma}|^2$, $T^e_{e\sigma} = (|t^{e\sigma}_{e\sigma}|^2 + |t^{e\bar{\sigma}}_{e\sigma}|^2)v^e_R/v^e_L$, $R^h_{e\sigma} = (|r^{h\sigma}_{e\sigma}|^2 + |r^{h\bar{\sigma}}_{e\sigma}|^2)v^h_R/v^e_L$, and $T^h_{e\sigma} = (|t^{h\sigma}_{e\sigma}|^2 + |t^{h\bar{\sigma}}_{e\sigma}|^2)v^h_R/v^e_L$, respectively, where $v^{e,h}_{L,R}$ are the velocities of the quasiparticles. The current conservation requires $R^e_{e\sigma} + T^e_{e\sigma} + R^h_{e\sigma} + T^h_{e\sigma} = 1$. We plot the probabilities of the four processes as a function of $k_\parallel$ for both spin-up and spin-down electron incidences in Fig. 5. In the $\mathcal{N} = 2$ region, the CAR dominates. Both spin channels participate in CAR; the sum of the CAR probabilities is greater than 1 or even close to 2, far greater than that under zero bias, as shown in the inset in Fig. 5(a). In the phases $\mathcal{N} = 0$ and $\mathcal{N} = 1$, AR and CAR are suppressed; the normal reflection and elastic cotunneling processes determine the transport. In Fig. 6, we plot the nonlocal conductance of the NM-NLSC-NM junction as a function of the bias. We can see that in the large-bias range, the conductance is much larger than the zero-bias conductance.

V. SUMMARY

In conclusion, we investigated the AR in a NLSC, including local AR in a NM-NLSC junction and CAR in a NM-NLSC-NM junction. Mapping the 3D NLSC to a 1D BDI class topological superconductor, two nontrivial phases, $\mathcal{N} = 1$ and 2, exist in the surface Brillouin zone. We showed that in both the nontrivial phases the MFs can lead to interesting spin transport. For the $\mathcal{N} = 1$ phase, a single MF couples to the electron with spin pointing in the $-y$ direction, independent of the wave vectors and other parameters, inducing equal-spin AR. For the $\mathcal{N} = 2$ phase, the two MFs induce resonant spin-flipped reflection, although they suppress ARs. Namely, when an electron is incident with spin $\mathbf{n}$ perpendicular to the y direction, a $-\mathbf{n}$ electron will be totally reflected. Both nontrivial phases can generate spin currents, but their spin polarizations are different. The polarizations of the spin currents induced in phases $\mathcal{N} = 1$ and 2 are antiparallel and perpendicular to the y axis, respectively. By using Zeeman fields, we can tune the spin currents with the two polarizations. We also studied transport in a NM-NLSC-NM junction and found that under finite bias, the fraction of CAR is greatly enhanced, far greater than in the zero-bias case, because all electrons participate in ARs.

ACKNOWLEDGMENTS

This work was supported by the National Natural Science Foundation of China under Grants No. 12074172 (W.C.), No. 12222406 (W.C.), No. 12264019 (W.L.), and No. 11864014 (X.W.); the Fundamental Research Funds for the Central Universities (W.C.); a startup grant at Nanjing University (W.C.); the Excellent Programme at Nanjing University; and the Ph.D. research startup foundation of Jiangxi University of Science and Technology (W.L.).

[1] A. Y. Kitaev, Phys. Usp. **44**, 131 (2001).
[2] F. Wilczek, Nat. Phys. **5**, 614 (2009).
[3] M. Z. Hasan and C. L. Kane, Rev. Mod. Phys. **82**, 3045 (2010).
[4] X. L. Qi and S. C. Zhang, Rev. Mod. Phys. **83**, 1057 (2011).
[5] J. Alicea, Rep. Prog. Phys. **75**, 076501 (2012).
[6] S. R. Elliott and M. Franz, Rev. Mod. Phys. **87**, 137 (2015).
[7] D. A. Ivanov, Phys. Rev. Lett. **86**, 268 (2001).
[8] J. Alicea, Y. Oreg, G. Refael, F. von Oppen, and M. P. A. Fisher, Nat. Phys. **7**, 412 (2011).
[9] R. M. Lutchyn, J. D. Sau, and S. Das Sarma, Phys. Rev. Lett. **105**, 077001 (2010).
[10] V. Mourik, K. Zuo, S. M. Frolov, S. Plissard, E. P. Bakkers, and L. P. Kouwenhoven, Science **336**, 1003 (2012).
[11] X.-L. Qi, T. L. Hughes, S. Raghu, and S.-C. Zhang, Phys. Rev. Lett. **102**, 187001 (2009).
[12] J. C. Y. Teo and C. L. Kane, Phys. Rev. Lett. **104**, 046401 (2010).
[13] T. Meng and L. Balents, Phys. Rev. B **86**, 054504 (2012).
[14] J. D. Sau and S. Tewari, Phys. Rev. B **86**, 104509 (2012).
[15] W. Wang, S. Kim, M. Liu, F. A. Cevallos, R. J. Cava, and N. P. Ong, Science **368**, 534 (2020).
[16] R. Nandkishore, Phys. Rev. B **93**, 020506(R) (2016).
[17] Y. Wang and R. M. Nandkishore, Phys. Rev. B **95**, 060506(R) (2017).
[18] S. Kobayashi, S. Sumita, Y. Yanase, and M. Sato, Phys. Rev. B **97**, 180504(R) (2018).
[19] P.-H. Fu, J.-F. Liu, and J. Wu, Phys. Rev. B **102**, 075430 (2020).
[20] W. Chen, L. Liu, W. Yang, D. Chen, Z. Liu, Y. Huang, T. Zhang, H. Zhang, Z. Liu, and D. W. Shen, Phys. Rev. B **103**, 035133 (2021).
[21] P. Rosenberg and E. Manousakis, Phys. Rev. B **104**, 134511 (2021).
[22] F. Zhou, Y. Liu, J. Wang, M. Kuang, T. Yang, H. Chen, X. Wang, and Z. Cheng, Phys. Rev. Mater. **5**, 074201 (2021).
[23] T. Shang, S. K. Ghosh, M. Smidman, D. J. Gawryluk, C. Baines, A. Wang, W. Xie, Y. Chen, M. O. Ajeesh, M. Nicklas, E. Pomjakushina, M. Medarde, M. Shi, J. F. Annett, H. Yuan, J. Ouintanilla, and T. Shiroka, npj Quantum Mater. **7**, 35 (2022).
[24] H. J. Kwon, K. Sengupta, and V. M. Yakovenko, Eur. Phys. J. B **37**, 349 (2004).
[25] L. Fu and C. L. Kane, Phys. Rev. B **79**, 161408(R) (2009).
[26] K. T. Law, P. A. Lee, and T. K. Ng, Phys. Rev. Lett. **103**, 237001 (2009).
[27] M. Wimmer, A. R. Akhmerov, J. P. Dahlhaus, and C. W. J. Beenakker, New J. Phys. **13**, 053016 (2011).
[28] S. B. Chung, X. L. Qi, J. Maciejko, and S. C. Zhang, Phys. Rev. B **83**, 100512(R) (2011).
[29] J. Wang, Q. Zhou, B. Lian, and S. C. Zhang, Phys. Rev. B **92**, 064520 (2015).
[30] J. J. He, T. K. Ng, P. A. Lee, and K. T. Law, Phys. Rev. Lett. **112**, 037001 (2014).
[31] J. J. He, J. Wu, T.-P. Choy, X.-J. Liu, Y. Tanaka, and K. T. Law, Nat. Commun. **5**, 3232 (2014).
[32] A. Haim, E. Berg, F. von Oppen, and Y. Oreg, Phys. Rev. Lett. **114**, 166406 (2015).
[33] N. F. Q. Yuan, Y. Lu, J. J. He, and K. T. Law, Phys. Rev. B **95**, 195102 (2017).
[34] X. Liu, X. Li, D.-L. Deng, X.-J. Liu, and S. Das Sarma, Phys. Rev. B **94**, 014511 (2016).
[35] L.-H. Hu, C. Li, D.-H. Xu, Y. Zhou, and F.-C. Zhang, Phys. Rev. B **94**, 224501 (2016).
[36] H.-H. Sun and J.-F. Jia, Sci. China: Phys. Mech. Astron. **60**, 057401 (2017).
[37] X.-H. Pan, X.-J. Luo, J.-H. Gao, and X. Liu, Phys. Rev. B **105**, 195106 (2022).
[38] H.-H. Sun, K.-W. Zhang, L.-H. Hu, C. Li, G.-Y. Wang, H.-Y. Ma, Z.-A. Xu, C.-L. Gao, D.-D. Guan, Y.-Y. Li, C. Liu, D. Qian, Y. Zhou, L. Fu, S.-C. Li, F.-C. Zhang, and J.-F. Jia, Phys. Rev. Lett. **116**, 257003 (2016).
[39] H.-H. Sun and J.-F. Jia, npj Quantum Mater. **2**, 34 (2017).
[40] S. Jeon, Y. Xie, J. Li, Z. Wang, B. A. Bernevig, and A. Yazdani, Science **358**, 772 (2017).
[41] A. P. Schnyder, S. Ryu, A. Furusaki, and A. W. W. Ludwig, Phys. Rev. B **78**, 195125 (2008).
[42] C.-K. Chiu, J. C. Y. Teo, A. P. Schnyder, and S. Ryu, Rev. Mod. Phys. **88**, 035005 (2016).
[43] W. Chen, K. Luo, L. Li, and O. Zilberberg, Phys. Rev. Lett. **121**, 166802 (2018).
[44] S. Tewari and J. D. Sau, Phys. Rev. Lett. **109**, 150408 (2012).
[45] C. L. M. Wong and K. T. Law, Phys. Rev. B **86**, 184516 (2012).
[46] Y. Yang, H. Li, L. Sheng, R. Shen, D. Sheng, and D. Xing, New J. Phys. **15**, 083042 (2013).
[47] M. Ezawa, Y. Tanaka, and N. Nagaosa, Sci. Rep. **3**, 2790 (2013).
[48] P. G. de Gennes, *Superconductivity of Metals and Alloys* (Benjamin, New York, 1966).
[49] C. W. Groth, M. Wimmer, A. R. Akhmerov, and X. Waintal, New J. Phys. **16**, 063065 (2014).
[50] R. J. Soulen, Jr., J. M. Byers, M. S. Osofsky, B. Nadgorny, T. Ambrose, S. F. Cheng, P. R. Broussard, C. T. Tanaka, J. Nowak, J. S. Moodera, A. Barry, and J. M. D. Coey, Science **282**, 85 (1998).
[51] C. Visani, Z. Sefrioui, J. Tornos, C. Leon, J. Briatico, M. Bibes, A. Barthélémy, J. Santamaría, and J. E. Villegas, Nat. Phys. **8**, 539 (2012).
[52] R. Cai, Y. Yao, P. Lv, Y. Ma, W. Xing, B. Li, Y. Ji, H. Zhou, C. Shen, S. Jia, X. C. Xie, I. Žutić, Q.-F. Sun, and W. Han, Nat. Commun. **12**, 6725 (2021).
[53] S. Bhandari, G.-H. Lee, K. Watanabe, T. Taniguchi, P. Kim, and R. M. Westervelt, Nano Lett. **20**, 4890 (2020).